Contents lists available at ScienceDirect

Colloids and Surfaces B: Biointerfaces

journal homepage: www.elsevier.com/locate/colsurfb

The influence of mannose-based esters on the mesophase behaviour of lyotropic liquid crystalline nanosystems as drug delivery vectors

Mattia Tiboni [a],[1], Paola Astolfi [b],[1], Michele Verboni [a], Serena Benedetti [a], Elisabetta Giorgini [c], Valentina Notarstefano [c], Francesco Vita [b], Simone Ranieri [b], Andrea Duranti [a], Simone Lucarini [a], Luca Casettari [a], Michela Pisani [b],[*]

[a] *Department of Biomolecular Sciences – DISB, University of Urbino Carlo Bo, Piazza del Rinascimento, 6, I-61029 Urbino, PU, Italy*
[b] *Department of Science and Engineering of Materials, Environment and Urban Planning – SIMAU, Polytechnic University of Marche, Via Brecce Bianche 12, I-60131 Ancona, Italy*
[c] *Department of Life and Environmental Sciences – DISVA, Polytechnic University of Marche, Via Brecce Bianche 12, I-60131 Ancona, Italy*

ARTICLE INFO

ABSTRACT

Lyotropic Liquid Crystalline (LLC) nanoparticles represent an emerging class of smart, biocompatible, and biodegradable systems for the delivery of drugs. Among these, structures with complex 3D architectures such as cubosomes are of particular interest. These are non-lamellar assemblies having hydrophobic and hydrophilic portions able to carry drugs of different nature. They can further be modulated including suitable additives to control the release of the active payload, and to promote an active targeting. Starting from monoolein (GMO) cubic phase, different concentrations of mannose-based esters were added, and the eventual structural modifications were monitored to ascertain the effects of the presence of glycolipids. Moreover, the structural properties of these nanosystems loaded with Dexamethasone (DEX), a very well-known anti-inflammatory steroid, were also studied. Experiments were carried out by synchrotron Small Angle X-ray Scattering (SAXS), Raman Microspectroscopy (RMS) and Attenuated Total Reflectance-Fourier Transform Infrared (ATR-FTIR) measurements. The drug delivery potential (*i.e.* entrapment efficiency and release properties) of the obtained nanoparticles was evaluated. Finally, *in vitro* cytocompatibility and anti-inflammatory activity studies of the prepared formulations were carried out. Inclusion of mannose-based surfactants up to 10 mol% influenced the structural parameters of *Im3m* cubic phase and swollen cubic phases were obtained with the different glycolipids with lattice parameters significantly higher than GMO. A complete cytocompatibility and an increased DEX activity were observed, thus suggesting the possibility to use GMO/glycolipids nanoparticles to formulate innovative drug delivery systems.

1. Introduction

Innovative drug delivery systems (DDS) have fascinated formulation scientists during the last decades. Among them, lipid-based vesicles such as liposomes have been the most studied in drug delivery presenting bilayer leaflets surrounding an aqueous core with the potentiality to carry both hydrophilic and hydrophobic payloads [1,2]. Recently, lyotropic liquid crystalline (LLC) mesophases (*e.g.*, hexagonal and cubic) received great attention for their possible use in the delivery of active ingredients such as peptides, proteins, genetic materials, and small molecules [3–7]. Compared to the lamellar phase typical of liposomes, the cubic structure represents a more exotic membrane phase that

consists of a single, continuous bilayer draped over an infinite periodic minimal surface (IPMS) that divide the space into two interpenetrating but unconnected networks. Among the potential reverse cubic phases that can be formed, it is possible to identify the Schwarz diamond (D, *Pn3m*), primitive (P, *Im3m*), and Schoen gyroid (G, *Ia3d*) minimal surfaces [8]. Glyceryl monooleate (monoolein, GMO) is one of the most employed lipids in the manufacture of bicontinuous cubic phases [9]. It is a biodegradable and biocompatible material included in the FDA inactive ingredients [10]. GMO, in water excess conditions and in the presence of a steric stabilizer, forms dispersed mesophases commonly known as cubosomes which typically have dimensions comprised between 100 and 200 nm and hence suitable for drug delivery purposes;

---

moreover, they are characterized by a large lipid-water interfacial area (*ca.* 400 m^{2}g^{-1}) [11] which allows the encapsulation and the protection of higher amounts of both hydrophilic and hydrophobic drugs [12] and also their more sustained release compared to liposomes. Another attractive feature of these systems is represented by the fact that their composition and structure can be modified according to their application by including in the formulation other excipients that may affect the mesophase and the dimensions of the water channels [5,13,14]. Among these, sugar-based esters or glycolipids can be considered with a particular interest since different biological pathways that include cell interactions (*e.g.*, signaling, recognition and adhesion) involve glycans or glycolipids present on cell surface [15,16]. Glycolipids are renewable, and functional non-ionic surfactants, able themselves to self-assemble in lyotropic phases [17–20]. An increased attention in the pharmaceutical field is currently devoted to these systems since they can act as permeation enhancers, wound healing promoters and active targeting excipient by exploiting the presence of sugar moieties on the surface of nano-sized DDS such as liposomes and niosomes [21–29]. In fact, by the interaction between sugar-based nanoparticles and specific sugar receptors present on specific cell membranes it is possible to release the drug payload specifically where needed.

In this work, we studied the phase behavior of GMO when coformulated, at different concentrations (*i.e.*, 10 and 30 mol%), with a particular family of mannose-based esters. The obtained nanoparticles, decorated on their surface with sugars molecules, could represent a drug delivery system able to load hydrophilic and hydrophobic molecules, to guarantee a controlled drug delivery and, above all, to enhance the drug therapeutic index by improving the delivery efficacy and increasing the cell compatibility [30]. In our previous study [21], this type of excipients has been used to formulate sugar decorated liposomes loaded with berberine hydrochloride with increased uptake from breast cancer cells, good biocompatibility, controlled release of the payload over time, and great stability. This time, as model drug we chose dexamethasone (DEX), a very well-known anti-inflammatory steroid used for the treatment of different inflammatory diseases, including autoimmune diseases, allergies, and cancer. Nevertheless, DEX usage is often restricted due to its poor water solubility; in addition, the prolonged systemic administration of DEX may cause severe side effects, such as hypertension, hyperglycemia, and intestinal bleeding [31]. Therefore, the controlled delivery of DEX is desirable.

After the sustainable enzyme-based synthesis and chemical characterization of the mannose-based surfactants (*i.e.*, chain length C10, C14, C18w), they were used at different concentrations (*i.e.*, 10 and 30 mol%) to formulate GMO-based DDSs both as bulk gel phase and as colloidal dispersions: the former were characterized by Small Angle X-Ray Scattering (SAXS) together with Raman Microspectroscopy (RMS) and Attenuated Total Reflectance - Fourier Transform Infrared (ATR-FTIR) measurements, and the latter were studied in terms of size, polydispersity index (PDI), and zeta potential. Moreover, drug loading and release studies were conducted to evaluate the drug delivery potential of obtained nanoparticles. Finally, *in vitro* cytocompatibility and antiinflammatory activity studies were carried out to explore the potential application of the mannose functionalized nanoparticles as therapeutics.

2. Materials and methods

2.1. Materials

Capric and oleic acids were bought from Fluorochem (Hadfield, UK); myristic acid and D-mannose from TCI (Zwijndrecht, Belgium); dexamethasone (DEX) and Pluronic® F127 (PEO$_{98}$-PPO$_{67}$-PEO$_{98}$), Novozyme 435 (lipase acrylic resin from *Candida antarctica*) (Novozyme), all organic solvents and molecular sieves MS 0.4 Å (powder and beads) from Sigma-Aldrich (Milan, Italy). Monomuls® 90-O18 (GMO), a glyceryl monooleate-based product similar to other commercial GMO formulations [8], was kindly provided by BASF (Germany).

Acetone was dehydrated with MS 4 Å beads. Compounds' structures were identified by combined ESI-MS, ^{1}H NMR, and ^{13}C NMR. A Waters Micromass ZQ spectrometer was employed to acquire ESI-MS spectra in a negative or positive mode using nebulizing nitrogen gas at 400 L/min and a temperature of 250 °C, cone flow 40 mL/min, capillary 3.5 kV, and cone voltage 60 V; only molecular ions [M-H]$^-$, [M+NH$_4$]$^+$ or [M+Na]$^+$ are given. ^{1}H NMR and ^{13}C NMR spectra, obtained from two Bruker AC 400 and 101 spectrometers, respectively, were analysed with the TopSpin 1.3 software package. Chemical shifts were measured by using the central peak of the solvent. Column chromatography purifications were performed under "flash" conditions using Merck 230–400 mesh silica gel. TLC was performed on Merck silica gel 60 F254 plates, which were visualized by exposure to ultraviolet light and to an aqueous solution of ceric ammonium molybdate.

2.2. Methods

2.2.1. General procedure for the synthesis of 6-O-acylmannose esters (3a−c – Scheme 1)

Novozyme 435 (0.200 g) and MS 4 Å (0.400 g) were added to a solution of the appropriate fatty acid (**1a–c**) (2.1 mmol) and D-mannose (**2**) (0.126 g, 0.7 mmol) in dry acetone (4.2 mL) [32]. The mixture was stirred at room temperature for 96 h, filtered, and the filtrate was concentrated. Purification of the residue by column chromatography (EtOAc/cyclohexane 4:1) gave **3a–c** as white spongy solids with an α/β anomeric ratio = 1:0.5. .

6-O-Decanoyl-D-mannopyranose (mannose caprate, URB1390) (3a, MC10) [33]. Yields, ^{1}H NMR and ^{13}C NMR data were previously reported [34]. ESI-MS: 333 [M-H]$^-$, 352 [M+NH$_4$]$^+$, 357 [M+Na]$^+$.

6-O-Tetradecanoyl-D-mannopyranose (mannose myristate, URB1391) (3b, MC14) [33]. Yields, ^{1}H NMR and ^{13}C NMR data were previously reported [34]. ESI-MS: 425 [M-H]$^-$, 444 [M+NH$_4$]$^+$, 449 [M+Na]$^+$.

6-O-Octadec-9Z-enoyl-D-mannopyranose (mannose oleate, URB1425) (3c, MC18w) [35]. Yield: 65%. ESI-MS: 443 [M-H]$^-$, 462 [M+NH$_4$]$^+$, 467 [M+Na]$^+$. ^{1}H NMR (DMSO-*d*$_6$): δ = 0.86 (t, 3 H + 1.5 H, *J* = 7.0 Hz, CH$_3$), 1.21–1.34 (m, 20 H + 10 H), 1.47–1.55 (m, 2 H + 1 H, OCCH$_2$*CH$_2$*), 1.96–2.03 (m, 4 H + 1 H, *CH$_2$*CH=CH*CH$_2$*), 2.25–2.30 (m, 2 H + 1 H, OC*CH$_2$*CH$_2$), 3.22–3.33 (m, 0.5×3H, H$^{3\beta}$, H$^{4\beta}$, H$^{5\beta}$), 3.35–3.40 (m, 1 H, H$^{4\alpha}$), 3.52–3.56 (m, 2 H + 0.5 H, H$^{2\alpha}$, H$^{3\alpha}$, H$^{2\beta}$), 3.70 (ddd, 1 H, $J_{H5\alpha-H6b\alpha}$ = 1.5 Hz, $J_{H5\alpha-H6a\alpha}$ = 7.0 Hz, $J_{H5\alpha-H4\alpha}$ = 9.0 Hz, H$^{5\alpha}$), 3.94–4.01 (m, 1 H + 0.5 H, H$^{6a\alpha}$, H$^{6a\beta}$), 4.27–4.32 (m, 1 H + 0.5 H, H$^{6b\alpha}$, H$^{6b\beta}$), 4.56–4.60 (m, 1 H + 1 H, OH$^{3\alpha}$, H$^{1\beta}$, OH$^{2\beta}$), 4.63 (d, 1 H, $J_{OH3\alpha-H3\alpha}$ = 4.0 Hz, OH$^{3\alpha}$), 4.68 (d, 0.5 H, $J_{OH3\beta\,-H3\beta}$ = 5.5 Hz, OH$^{3\beta}$), 4.85 (dd, 1 H, $J_{H1\alpha-H2\alpha}$ = 1.0 Hz, $J_{H1\alpha-OH1\alpha}$ = 4.5 Hz, H$^\alpha$) 4.90 (d, 1 H, $J_{OH4\alpha\,-H4\alpha}$ = 6.0 Hz, OH$^{4\alpha}$), 4.95 (d, 0.5 H, $J_{OH4\beta-H4\beta}$ = 5.0 Hz, OH$^{4\beta}$), 5.27–5.28 (m, 2 H + 1 H, CH=CH), 6.27 (d, 0.5 H, $J_{OH1\beta\,-H1\beta}$ = 8.5 Hz, OH$^{1\beta}$), 6.38 (d, 1 H, $J_{OH1\alpha-H1\alpha}$ = 4.5 Hz, OH$^{1\alpha}$) ppm. ^{13}C NMR (DMSO-*d*$_6$): δ = 14.4 (1.5 C), 22.4 (0.5 C), 22.5 (1 C), 24.9 (1 C), 25.7 (0.5 C), 27.0 (1.5 C), 27.1 (1.5 C), 28.9 (1 C), 29.0 (1 C), 29.06 (1 C), 29.09 (1 C), 29.14 (1.5 C), 29.18 (0.5 C), 29.21 (0.5 C) 29.3 (1 C), 29.4 (0.5 C), 29.48 (0.5 C), 29.51 (0.5 C), 29.6 (2 C), 31.4 (0.5 C), 31.7 (1 C), 33.86 (0.5 C), 33.91 (1 C), 64.66 (C6, 0.5 C), 64.71 (C6, 1.0 C), 67.3 (C5, 0.5 C), 67.6 (C5, 1 C), 70.8 (C4, C3 2 C), 71.8 (C2, 1 C), 71.9 (C2, 0.5 C), 74.0 (C4, 0.5 C), 74.5 (C3, 0.5 C), 94.5 (C1, 1 C), 94.6 (C1, 0.5 C), 128.2 (CH=CH, 0.5 C), 130.1 (CH=CH, 2 C), 130.2 (CH=CH, 0.5 C), 173.4 (CO, 1.5 C) ppm.

2.2.2. Preparation of blank and drug-loaded non-dispersed lipid phases

Unloaded LLC structures were obtained, in bulk phase, by dissolving 25 mg of monoolein (*GMO*) or 25 mg of a mixture GMO + 10 mol% (*10MC10, 10MC14* and *10MC18w*) or GMO + 30 mol% (*30MC10, 30MC14* and *30MC18w*) mannose-based esters in chloroform and adding Pluronic® F127 (10% w/w of lipid) to the same solvent. The solvent was removed by evaporation, first under nitrogen flow and subsequently under vacuum. 250 μL of water were added, and the mixture was left
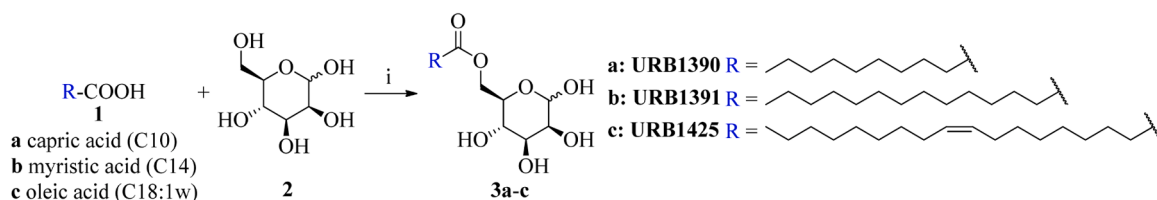
Scheme 1. Reagents and conditions: (i) Novozyme 435, MS 4 Å, dry acetone, rt, 96 h.

equilibrating at room temperature for 24 h thus obtaining a homogeneous gel phase. In the following, the acronyms GMO and 10MCX or 30MCX, where X is 10, 14 or 18w, will be used to indicate the unloaded samples. DEX loaded bulk LLC phases were prepared as described for the empty ones but including 2 mg of DEX as model drug in the chloroform lipid/F127 mixtures. To indicate the loaded samples the prefix *DEX@* will be added to the codes described above.

2.2.3. Preparation of nanostructured GMO dispersions

LLC dispersions (10 mg/mL lipid concentration) were obtained by adding the proper volume of water to the previously prepared gels and by probe sonicating (Sonic Vibracell) for 10 min in pulse mode (1 s pulse interrupted by 1 s break, 50% maximum power) All samples were stored at room temperature.

2.2.4. SAXS measurements

SAXS experiments were carried out at the SAXS beamline of Elettra Sincrotrone Trieste (Italy) to investigate the prepared LLC mesophases. A wavelength $\lambda = 1.54$ Å (8 keV incident beam energy) and a q range of 0.1–5 nm^{-1} were used. A Dectris Pilatus 1 M detector was employed to record 2-D X-ray diffraction patterns which were integrated into 1-dimensional plots of the scattering intensity (I) *versus* the scattering vector (q), with the latter defined as $q = 4\pi\sin\theta/\lambda$ (with 2θ being the scattering angle) and calibrated against a silver behenate standard ($d = 5.83$ nm). The lattice parameter (a) of cubic phases was obtained through a linear fit of q_{hkl} *vs* $\sqrt{h^2 + k^2 + l^2}$, with $q_{hkl} = \frac{2\pi}{a}\sqrt{h^2 + k^2 + l^2}$ indicating the q value of the *hkl* reflection for a cubic lattice. In a similar fashion, the d spacing of L_α lamellar phases was obtained by fitting $q_h = \frac{2\pi}{d}h$, the q value of the h-th order reflection, against h.

2.2.5. ATR-FTIR measurements

The infrared analysis was performed at the Advanced Research Instrumentation Laboratory - Polytechnic University of Marche (Ancona, Italy) and at the SISSI beamline, Elettra Sincrotrone Trieste (Italy). ATR-FTIR spectra were acquired by a Platinum ATR accessory mounting a diamond crystal and coupled with a Bruker INVENIO-R interferometer and a Deuterated TriGlycine Sulfate (DTGS) detector (Bruker Optics, Ettlingen, Germany). 10 µL of each sample were deposited onto the clean diamond crystal and ATR-FTIR spectra were collected at room temperature, every 10 s; sample dehydration was checked by the disappearance of the combination band at ~2100 cm^{-1}, assigned to the vibrational modes of water. The following setup was used for all the samples and also for background: 4000–800 cm^{-1} spectral range, 128 scans, and 4 cm^{-1} spectral resolution. The experiment was performed in triplicate.

Raw spectra were submitted to Atmospheric Compensation and Vector Normalization routines and then interpolated in the 1830–800 cm^{-1} spectral range (OPUS 7.5, Bruker Optics, Ettlingen, Germany).

2.2.6. RMS measurements

Raman spectra were collected by an XploRA Nano Raman Microspectrometer (Horiba Scientific) at the Advanced Research Instrumentation Laboratory - Polytechnic University of Marche (Ancona, Italy).

10 µL of each sample were deposited onto a glass support and then, the Raman spectra were acquired according to the following setup: 200–1800 cm^{-1} spectral range, 532 nm or 785 nm laser diode, 600 lines per mm grating. Spectra were dispersed onto a 16-bit dynamic range Peltier-cooled CCD detector; the spectrometer was calibrated to the 520.7 cm^{-1} line of silicon prior to spectral acquisition. Raw Raman spectra were submitted to polynomial baseline correction and vector normalisation, to reduce noise and enhance spectrum quality (Labspec 6 software, Horiba Scientific).

2.2.7. Particle size and zeta potential measurements

A Malvern Zetasizer Nano ZS (Malvern Instruments GmbH) with Dispersion Technology Software V 5.03 was used to physically characterize the nanoparticle dispersions, through a measurement of the average particle diameter, the polydispersity index (PDI) and the zeta potential (Zp). Samples were properly diluted, measurements were repeated on three independent samples, and all data were averaged.

2.2.8. Encapsulation efficiency studies

To determine the encapsulation efficiency, a preliminary dialysis was carried out using (Spectra/Por® Float-A-Lyzer® G2 MWCO 10 kDa (Spectrum Lab, USA) dialysis tubes against 3 L of double distilled water for 30 mins to remove the non-encapsulated drug. The formulations were then moved into centrifugal filters (MWCO 10 kDa, VWR, USA) and centrifuged at 2500 G for 30 min. The filtered solutions were collected, and the non-encapsulated DEX analysed with HPLC.

The amount of encapsulated drug (EE%) was calculate using the following equation:

$$EE\% = \frac{drug_{tot} - drug_{ne}}{drug_{tot}} * 100$$

where $drug_{tot}$ is the total amount of DEX, encapsulated and non-encapsulated, and $drug_{ne}$ is the non-encapsulated DEX.

2.2.9. In vitro drug release studies

To evaluate the drug release from the prepared formulations, 1 mL of each formulation was put in a dialysis tube (Spectra/Por® Float-A-Lyzer® G2 MWCO 10 kDa, Spectrum Lab, USA) and placed in 50 mL of 50% EtOH kept at 37 °C under stirring. At determined timepoints (0.5, 1, 2, 4, 6, 24 h) 1 mL of the release medium was withdrawn and analysed with HPLC (1260 Infinity II, Agilent, USA) using a mixture of 0.5% formic acid in water and acetonitrile (ratio 60:40) as mobile phase, with a flow rate of 1 mL/min in an Agilent Poroshell 120 C18, 100 × 4.6 mm, 2.7 µm column (Agilent, USA). The injection volume was 20 µL and the detection signals were recorded at 242 nm at room temperature.

2.2.10. In vitro cytocompatibility on RAW 264.7

The cytotoxicity of the prepared formulations was investigated in RAW 264.7 cells (murine macrophages) cultured in DMEM medium supplemented with 10% fetal bovine serum, 1% penicillin/streptomycin 100 U/mL, 1% L-glutamine, and 1% sodium pyruvate (Sigma-Aldrich, Milan, Italy). Cells were seeded in 96-well plates (1×10^4 cells/well) and incubated for 24 h with the different drug loaded formulations at concentrations ranging from 50 to 200 µg/mL (DEX content from 4 to 16 µg/mL). The same concentrations of non-encapsulated DEX (from 4

to 16 μg/mL) were also tested. After treatment, the drug loaded formulations and free DEX were removed, and a fresh medium containing the WST-8 reagent (Sigma-Aldrich, Milan, Italy) was added to each well, as previously reported [36]. Cells were further incubated at 37 °C up to 2 h, and color development was monitored at 450 nm in a multiwell plate reader (Multiskan FC, Thermo Scientific). Data were expressed as cell viability (%) *vs* untreated control cells.

2.2.11. *In vitro anti-inflammatory activity on RAW 264.7 stimulated by lipopolysaccharide*

The anti-inflammatory properties of the drug-loaded formulations were evaluated in RAW 264.7 cells stimulated by lipopolysaccharide (LPS) (Sigma-Aldrich, Milan, Italy). Cells were seeded in 96-well plates (3 $\times 10^4$/well) and treated for 24 h with LPS (1 μg/mL) in the presence of the different drug-loaded formulations at the concentration of 50 μg/ mL (DEX content equal to 4 μg/mL). Non-encapsulated dexamethasone (4 μg/mL) was also tested as a reference. After incubation, nitric oxide (NO) release was determined in the culture medium by the Griess reagent (Sigma-Aldrich, Milan, Italy), as recently reported [37]. Briefly, 50 μL culture medium was added to 50 μL Griess (40 mg/mL) in a 96-well plate; after incubation for 10 min at room temperature in the dark, color development was measured at 540 nm in a multiwell plate reader (Multiskan FC, Thermo Scientific). Data were expressed as NO release (%) *vs* the positive control (LPS-treated cells). In the same set of experiments, RAW 264.7 cell viability in LPS-stimulated cells was monitored by the WST-8 assay as described above.

2.2.12. *Statistical analysis*

Comparisons between multiple means were performed *via* ANOVA followed by Tukey's *post hoc* test. Significance was set at $p < 0.05$. GraphPad Prism 6.0 (GraphPad Software, Inc., San Diego, CA, USA) was used for statistical analysis.

3. Results and discussion

3.1. *Mannose esters synthesis*

6-*O*-acylmannose esters (**3a−c**) were synthesized following a one-step enzymatic reaction procedure previously described [32]. Briefly, to have a regioselective esterification of the primary hydroxyl group of the D-mannose (**2**) with the opportune fatty acid (**1a−c**) suitable catalyst such as Novozyme was selected. Together with this, a water-free reaction environment created with anhydrous acetone and the presence of sieves was used. The reaction was monitored by TLC and HPLC-ESI-MS
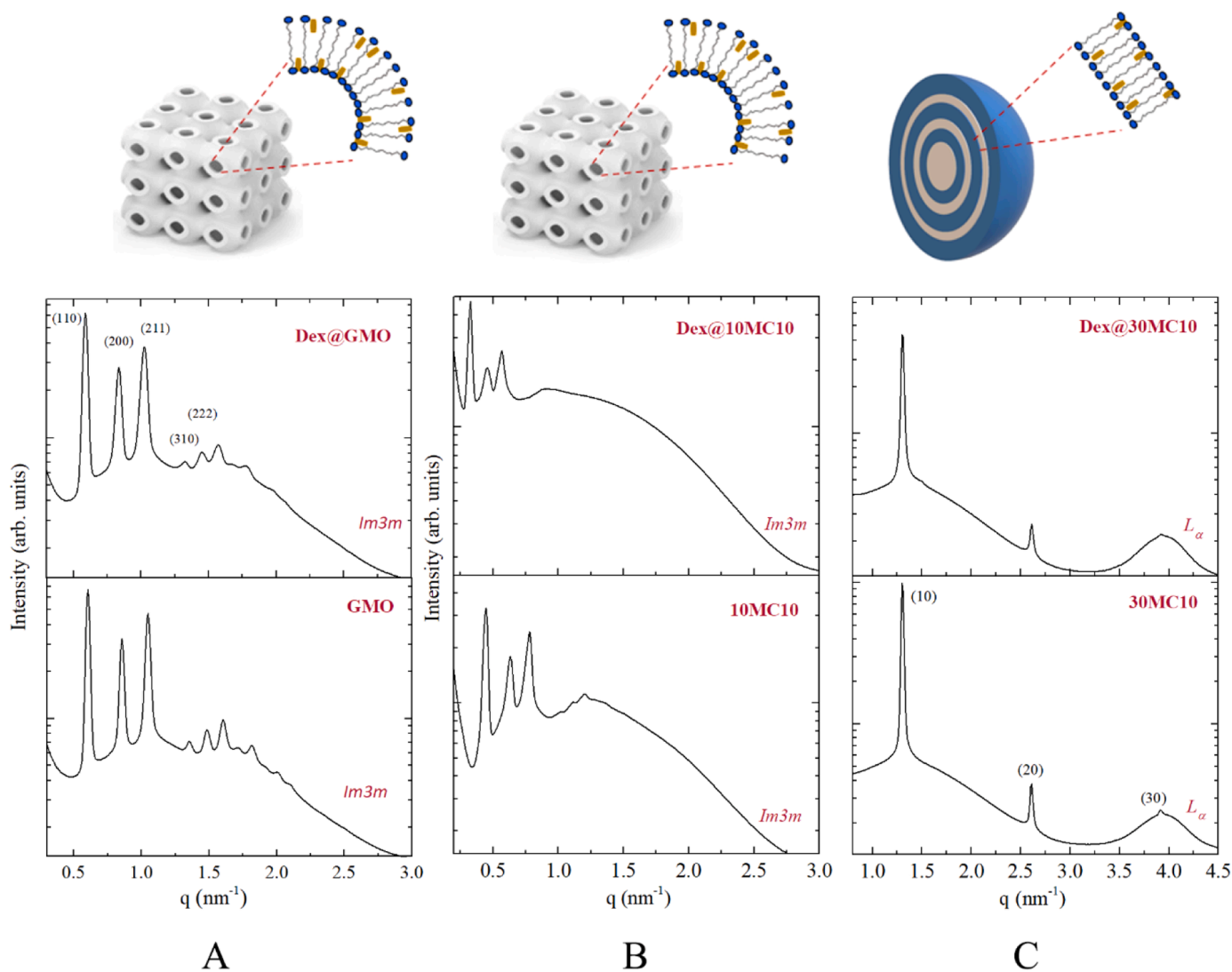

Fig. 1. SAXS diffraction profiles for (A) *GMO* and *DEX@GMO* bulk *Im3m* cubic phases; (B) *10MC10* and *DEX@ 10MC10 Im3m* cubic phase and (C) *30MC10* and *DEX@ 30MC10 L_α* lamellar phases. A schematic representation of the phase behaviour observed for the different mesophases with DEX incorporated (yellow dots) is reported above each system.

and no traces of other monoesters or diesters were detected. The same results were confirmed also by NMR analysis. NMR and ESI-MS characterization are reported in the supplementary material.

3.2. Characterization of bulk lipid phases

3.2.1. SAXS analysis

A systematic study on the phase behaviour of GMO/glycolipids mixtures as a function of the fatty acid chain length of the glycolipids (MC10, MC14, MC18w) and of their concentrations was carried out by means of SAXS. All systems were studied in excess aqueous solution and in presence of F127, since the same samples were also used as dispersed phases (see below).
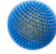
Fig. 1A shows the SAXS profiles for bulk phases of *GMO* and *DEX@GMO* evidencing in both cases an *Im3m* cubic lattice symmetry with Bragg peaks in the ratios $\sqrt{2} : \sqrt{4} : \sqrt{6} : \sqrt{8} : \sqrt{10}$ [38]. DEX encapsulation did not induce changes in the phase symmetry, but a slight increase in the unit cell from $a = 14.8$ nm to $a = 15.1$ nm was observed, likely due to the presence of DEX in the polar/apolar interface of GMO and hence to the decrease of the interfacial curvature.

Addition of 10 mol% of glycolipid MC10 to GMO matrix determined the formation of a swollen *Im3m* cubic phase with the lattice parameter a which increased from 14.8 nm to 20.0 nm, without changes in the cubic symmetry (Fig. 1B). The presence of MC10, characterized by a larger hydrophilic headgroup than GMO, resulted in a significant increase of the polar region and, consequently, in the change of the molecular wedge shape toward a more cylindrical one, but still characterized by a Critical Packing Parameter (CPP) > 1 [39]. This rearrangement leads to the formation of a cubic structure with a reduced negative interfacial curvature which resulted in a very large water channel radius (data shown in Table 1). Also in this case, upon encapsulation of the drug an increase in the unit cell was observed.

By increasing MC10 concentration in the GMO matrix to 30 mol%, a phase transition from *Im3m* to L_α, with lattice parameter $d = 4.8$ nm, occurred because of a further decrease in the interfacial curvature and of

a more cylindrical molecular shape (CPP $\approx$ 1). In this system, the presence of DEX had no effect on either the phase symmetry or lattice parameter (Fig. 1C).

When glycolipids MC14 and MC18w were included in the GMO matrix at 10 mol% concentration, *Im3m* cubic structures with unit cell $a = 17.5$ nm and 17.1 nm, respectively, were detected. Noteworthily, these lattice parameters are larger than GMO, because of the increased polar headgroup, but significantly smaller than that of GMO/MC10 matrix. In fact, the presence of these gliycolipids (MC14 with a C14 atoms saturated hydrocarbon chain and MC18w with a C18 atoms unsaturated hydrocarbon chain) could led to an increase of the effective volume of the amphiphile acyl chain, and hence also of the negative interfacial curvature, in this way partially balancing the increase of the hydrophilic region determined by the presence of the polar mannose groups. DEX loading determined, as in the previous systems, an increase of the unit cell parameters to $a = 21.4$ nm for *DEX@ 10MC10* and to $a = 17.9$ nm for *DEX@ 10MC18w*. A phase transition from the cubic *Im3m* to the lamellar L_α was observed when the two glycolipids were included in the formulation at 30 mol% concentration. In these cases, the unit cells were $d = 4.94$ nm for *30MC10* and $d = 4.98$ nm for *30MC18w* and remained unaffected upon DEX addition, since the drug molecule, as already hypothesized for the cubic structures, is likely included in the polar/apolar region without changes in the *d*-spacing.

The structural parameters for the studied systems are all reported in Table 1. The radii of water channels were estimated by using the relation:

$$r_w = \left[\left(-\sigma/2\pi\chi \right)^{(1/2)} a \right] - l$$

where l is the lipid length (*ca.* 1.7 nm) [40] and σ and χ are topological constants, characteristic of a given cubic phase (*Im3m* structures $\sigma = 2.345$ and $\chi = -4$).

3.2.2. ATR-FTIR and RMS analyses

The ATR-FTIR spectra of *DEX@GMO, DEX@ 10MC10, DEX@ 10MC14,* and *DEX@ 10MC18w* systems are shown in Fig. 2 (red line), together with those of the corresponding empty matrices (green line) and bare DEX (black line). The most representative bands in DEX spectrum are the following: 1703 cm^{-1} (stretching vibration of the C=O moiety); 1660 cm^{-1} (stretching vibration of the C=O moiety conjugated with C=C bonds); 1620 cm^{-1} and 1602 cm^{-1} (stretching vibration of conjugated C=C bonds); 1269 cm^{-1} (stretching vibration of the C-F bond); 1055 cm^{-1} (stretching vibration of the C-O moiety), and 892 cm^{-1} (bending vibration of the C-F bond) [41,42]. Interestingly, the bands at 1660 cm^{-1}, 1620 cm^{-1}, 1602 cm^{-1}, and 892 cm^{-1} of DEX are also evident in the spectra of the loaded systems, clearly confirming the encapsulation of the drug.

Moreover, a possible interaction between DEX and the lipid matrices may be suggested by a small shift displayed by the peaks at 1660 cm^{-1}, 1620 cm^{-1}, 1602 cm^{-1}, associated with the carbonyl group and the double bonds conjugated to it. Conversely, no shift was found for the vibrational mode at 892 cm^{-1} due to the axial deformation of the C-F bond. In Fig. 3, the Raman spectra of *DEX@GMO, DEX@ 10MC10, DEX@ 10MC14,* and *DEX@ 10MC18w* systems (red line) are shown, together with those of the corresponding empty matrices (green line) and bare DEX (black line).

The full Raman characterization of DEX was performed, and the most significant bands are the following: 680 cm^{-1} (in-plane bending vibration of C-C bonds) [43]; 765 cm^{-1} (vibration of C–F moiety) [44]; 926 cm^{-1}, 1150 cm^{-1} and 1185 cm^{-1} (bending vibrations of CH$_3$ and CH$_2$ groups) [45]; 1443 cm^{-1} (bending vibration of CH$_2$ groups) [46]; 1605 cm^{-1} (stretching vibration of conjugated C=C bonds) [46]; 1652 cm^{-1} (stretching vibration of the C=O moiety conjugated with C=C bonds) [46,47]; 1700 cm^{-1} (stretching vibration of the C=O moiety) [46]. Also in this case, some of DEX bands are present in the loaded samples, sometimes shifted at higher wavenumbers, as for the
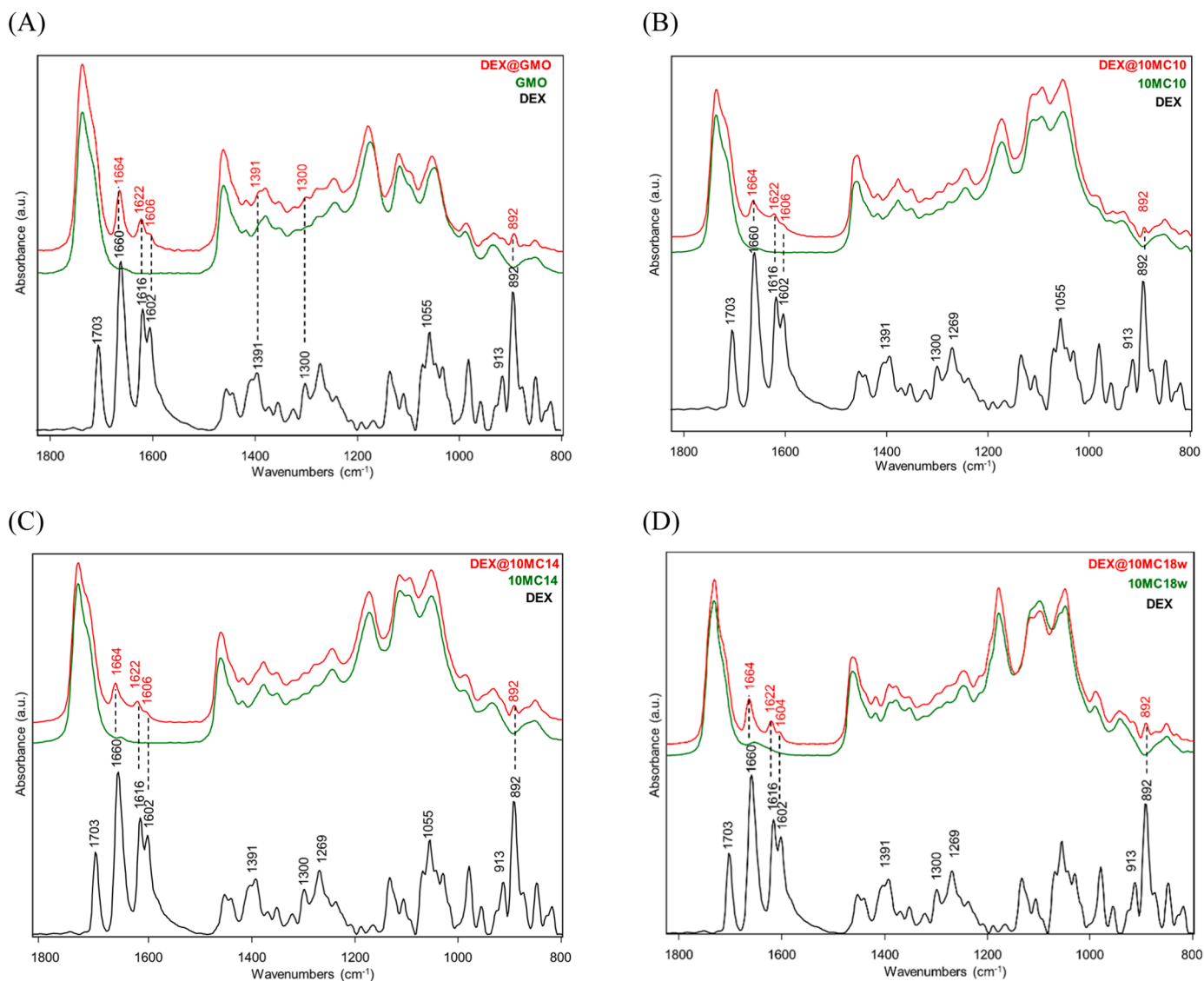
Table 1

Phase structure, lattice parameter (cubic phase: a; lamellar phase: d) and water channel radius (r_w) or water thickness (d_w) of GMO and GMO/glycolipids, for cubic phase and lamellar phase, respectively, empty and loaded with DEX.

	Phase	a or d (nm)	r_w or d_w (nm)
GMO	*Im3m*	14.8	2.80
DEX@GMO		15.1	2.90
10MC10	*Im3m*	20.0	4.40
DEX@ 10MC10		27.3	6.62
30MC10	L_α	4.80	1.37
DEX@ 30MC10		4.80	1.37
10MC14	*Im3m*	17.5	3.63
DEX@ 10MC14		21.4	4.82
30MC14	L_α	4.94	1.51
DEX@ 30MC14		4.94	1.51
10MC18w	*Im3m*	17.1	3.51
DEX@ 10MC18w		17.9	3.75
30MC18w	L_α	4.98	1.55
DEX@ 30MC18w		4.98	1.55

(A)

(B)

(C)

(D)

Fig. 2. ATR-FTIR spectra of: (A) *GMO* and *DEX@GMO*; (B) *10MC10* and *DEX@ 10MC10*; (C) *10MC14* and *DEX@ 10MC14*, and (D) *10MC18w* and *DEX@ 10MC18w*. In all figures, the spectrum of bare DEX (black line) is included for comparison. Spectra are shown in the 1830–800 cm^{-1} range in absorbance mode and are shifted along y-axis for a better comprehension.

1652 cm^{-1} DEX band, confirming a possible interaction between DEX and the lipid matrix.

3.3. Characterization of dispersed lipid phases

3.3.1. Size and zeta potential

All the formulated DDS (empty and DEX-loaded) have a monomodal size distribution and low PDI values as reported in Table 2. The mean particle sizes for the empty systems are in the range 110–140 nm with cubosomes (GMO and 10MC) and slightly smaller with liposomes (30MC).

Upon DEX encapsulation, a small increase in the nanoparticles dimensions is generally observed probably due to the effective incorporation of the drug into the nanosystem as already reported in other studies [48].

The zeta potential values of the prepared nanoparticles are slightly negative in all cases even if both GMO and glycolipids are neutral [38].

3.3.2. Entrapment efficiency

Very high value (95–98%) were obtained for the entrapment efficiency of DEX in all the studied systems as shown in Table 2. No

significant differences were observed between the various systems according to the nature of the glycolipid and to its concentrations. DEX is a moderate lipophilic molecule, as suggested by its LogP value of 1.83 [49], and for this reason it is efficiently encapsulated in the lipid matrices where it finds a suitable environment.

3.3.3. In vitro drug release studies

In vitro drug release behaviour of DEX from the different prepared formulations was studied and the release profiles are shown in Fig. 4. As release medium, a 50% v/v ethanolic solution was selected to increase the DEX solubility and maintain sink conditions. The release profiles from cubic structures formed with glycolipids at 10 mol% (Fig. 4A) showed a 71.4 ± 0.4% (*DEX@GMO*), 78.3 ± 2.7% (*DEX@10MC10*), 80.8 ± 0.7% (*DEX@10MC14*), and 90.0 ± 3.8% (*DEX@10MC18w*) release of DEX during the first 6 h with a plateau to 24 h. The highest release was observed for the *DEX@ 10MC18w* system which may be seen as the most fluid one with the hydrocarbon chains composed only by unsaturated C18 acyl residues and this likely favours the drug release. Moreover, compared to *DEX@GMO*, which should have the same fluidity, *DEX@ 10MC18w* cubic structure has a larger water channel radius and this could favour the release as well. A similar behaviour was
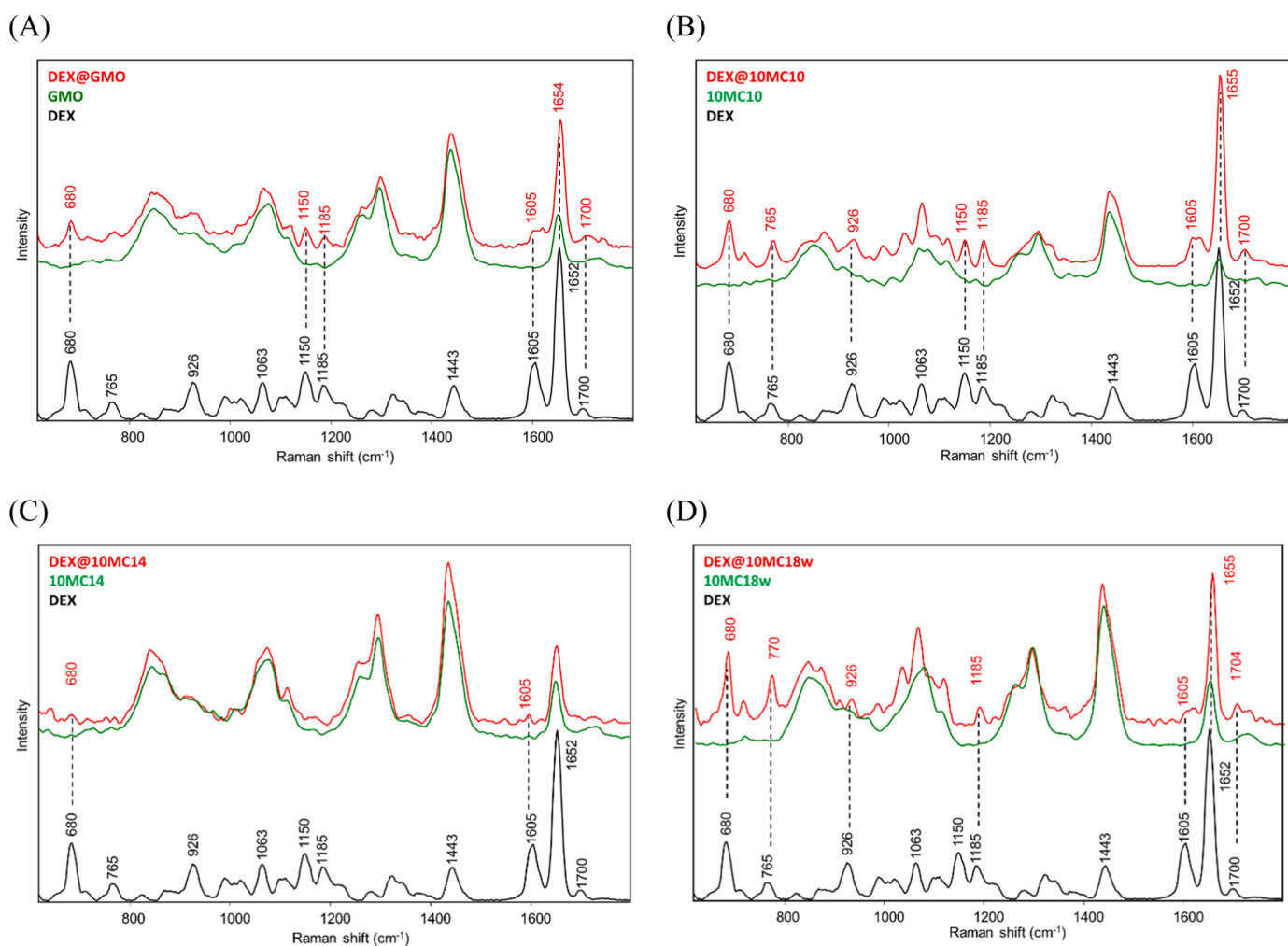
(A)

(B)

(C)

(D)

Fig. 3. Raman spectra of: (A) *GMO* and *DEX@GMO*; (B) *10MC10* and *DEX@ 10MC10*; (C) *10MC14* and *DEX@ 10MC14*, and (D) *10MC18w* and *DEX@ 10MC18w*. In all figures, the spectrum of bare DEX (black line) is included for comparison. Spectra are showed in the 600–1800 cm^{-1} range and are shifted along y-axis for a better comprehension.

Table 2
Average particle size (Z$_{ave}$), Polydispersity index (PDI), Zeta potential (Zp) and Entrapment efficiency of the formulated DDs.

Sample	Z$_{ave}$ (nm)	PDI	Zp	EE%
GMO	132.4 ± 2.8	0.15 ± 0.03	-22.5 ± 2.4	——
DEX@GMO	136.7 ± 2.8	0.16 ± 0.01	-24.9 ± 1.2	97.2 ± 1.1
10MC10	102.0 ± 1.7	0.13 ± 0.01	-24.2 ± 3.2	——
DEX@ 10MC10	137.4 ± 2.4	0.09 ± 0.02	-24.9 ± 0.9	95.4 ± 0.8
30MC10	80.3 ± 1.8	0.24 ± 0.02	-17.4 ± 2.0	——
DEX@ 30MC10	85.8 ± 2.4	0.16 ± 0.02	-18.4 ± 1.6	96.3 ± 1.9
10MC14	120.6 ± 2.2	0.10 ± 0.03	-24.9 ± 0.9	——
DEX@ 10MC14	135.6 ± 3.2	0.09 ± 0.02	-25.0 ± 1.0	96.7 ± 2.1
30MC14	105.8 ± 1.8	0.07 ± 0.02	-13.9 ± 0.7	——
DEX@ 30MC14	122.0 ± 3.4	0.12 ± 0.02	-13.4 ± 2.0	98.3 ± 1.3
10MC18w	106.2 ± 3.5	0.13 ± 0.02	-22.0 ± 2.1	——
DEX@ 10MC18w	117.8 ± 2.0	0.20 ± 0.01	-21.3 ± 0.4	98.1 ± 1.5
30MC18w	109.4 ± 1.8	0.21 ± 0.08	-20.4 ± 0.7	——
DEX@ 30MC18w	114.0 ± 6.2	0.33 ± 0.09	-22.6 ± 1.6	98.2 ± 1.2

observed also with the liposomes obtained when glycolipids were added at 30 mol% (Fig. 4B); in fact, most of the drug was released in 6 h but with some differences: 71.3 ± 3.1% (*DEX@30MC10*), 79.7 ± 1.6% (*DEX@30MC14*), and 96.3 ± 2.8% (*DEX@30MC18w*). Even in this case, it is possible to suppose that the presence of an unsaturation in the acyl chain of the MC18w forms a more fluid membrane that allow a faster and higher drug release. Moreover, slight differences in the release

profiles between cubosomes and liposomes can be observed, with release from liposomes being a little bit faster than from cubosomes. This behaviour could be justified by their different internal structures with cubosomes having a more intricated water channels network.

3.3.4. In vitro cytocompatibility and anti-inflammatory effect on RAW 264.7

The cytocompatibility of the DEX loaded formulations was evaluated on RAW 264.7 cells. The DDSs showed an increasing cytotoxicity at the concentrations of 100 and 200 μg/mL (corresponding to a DEX content of 8 and 16 μg/mL). The drug alone at the tested concentrations resulted cytocompatible suggesting a cytotoxicity deriving from the excipients. No significant decrements of cell viability were observed with the 50 μg/mL DEX loaded samples (Fig. 5 A). For this reason, the 50 μg/mL concentration was chosen to test the anti-inflammatory activity using RAW 264.7 stimulated with LPS as inflammatory model.

The anti-inflammatory tests were performed to evaluate the effective activity of the DEX encapsulated in the cubic and liposomal delivery systems. The stimulation of RAW 264.7 cells by LPS (CTR+) led to a strong extracellular release of NO as an inflammatory response mediator in comparison to unstimulated cells (CTR-) (Fig. 5B). When cells were stimulated with LPS in the presence of 50 μg/mL of the DEX loaded formulations or free DEX, a significant decrease of NO production was observed. Noteworthily, the reduction of NO release by the DDSs was significantly different as compared to non-encapsulated DEX. This
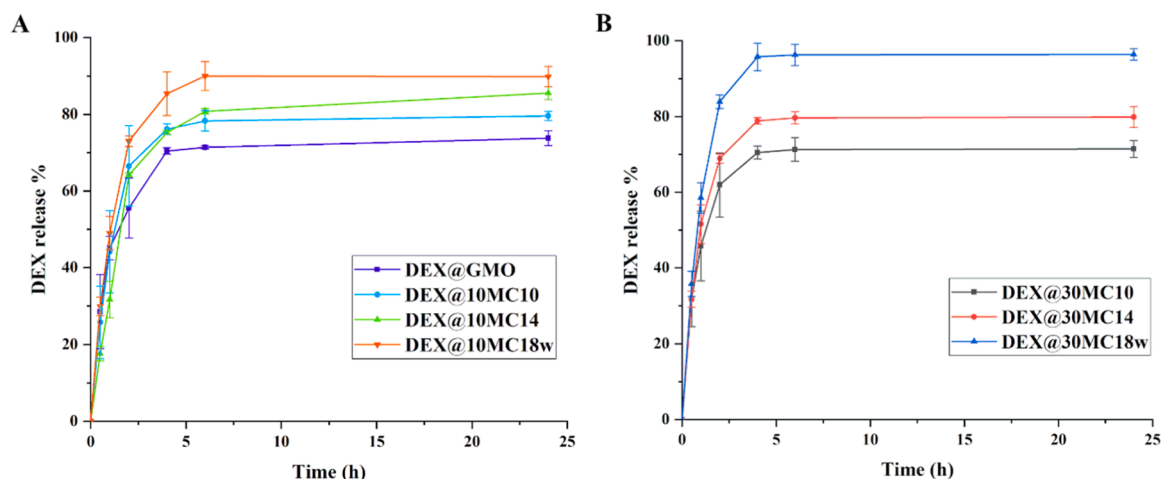
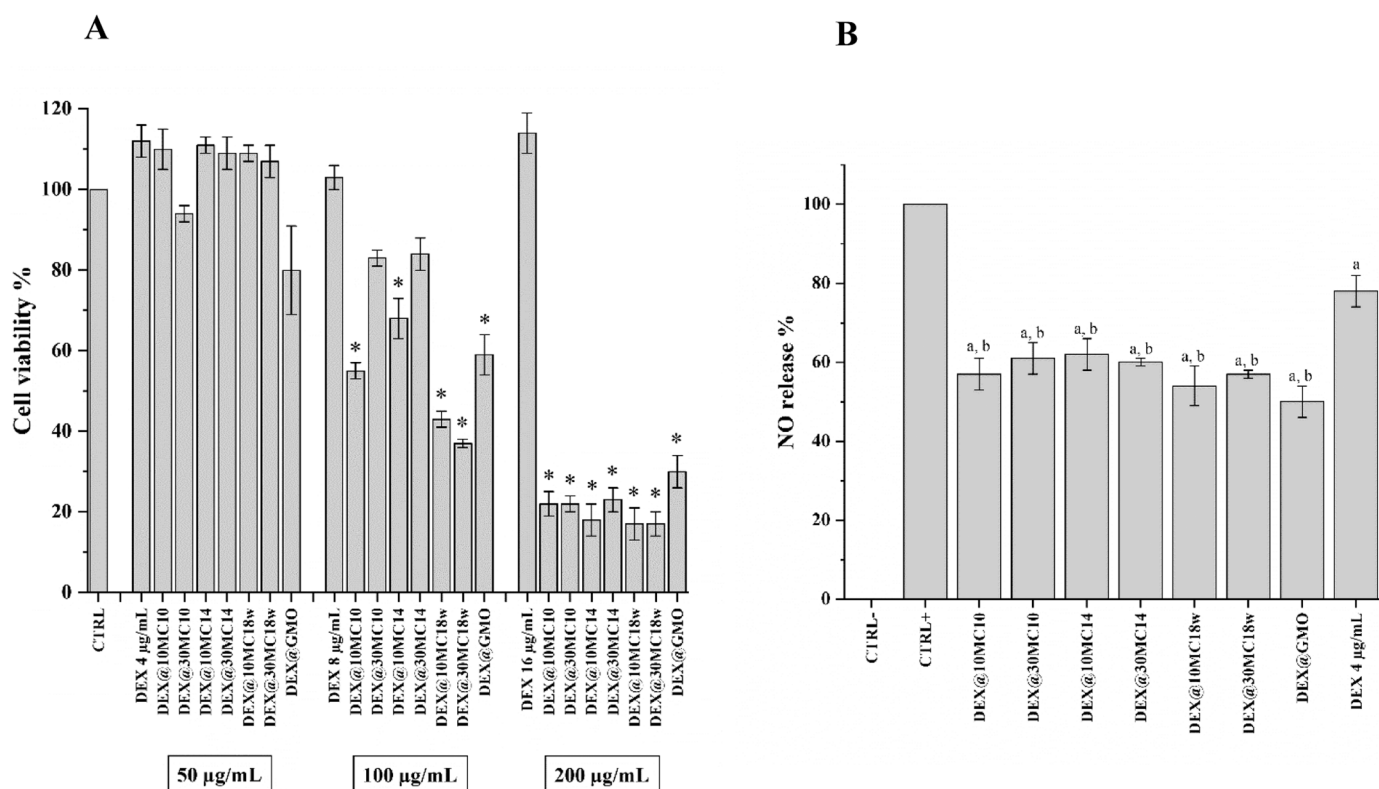**Fig. 4.** *In vitro* drug release studies in 50% ethanol solution.

Fig. 5. (A) RAW 264.7 cell viability (% *vs.* CTR) after 24-h treatment with increasing concentrations of DEX loaded systems (50–200 μg/mL) or free DEX (4–16 μg/mL). (*) significantly different from untreated control cells (Tukey post-hoc test). Data are reported as the mean ± SD (n = 3). (B) Extracellular NO release (% *vs.* CTR+) after stimulation of RAW 264.7 cells by 1 μg/mL LPS for 24 h in the presence of 50 μg/mL DEX loaded formulations or free DEX (4 μg/mL). (a) significantly different from the positive control; (b) significantly different from dexamethasone (Tukey post-hoc test). Data are reported as the mean ± SD (n = 3). CTR-: negative control (unstimulated cells).

behaviour could be attributed to the sustained release properties of the formulated DDSs. Differences in NO release between the seven different tested formulations were not significant indicating that the cubic phases had an activity comparable with the well-established liposomal phase. Even the length of the acyl chain of the sugar esters, considered in this work, did not affect the anti-inflammatory activity suggesting that, the modification of the hydrophobic tail of this type of surfactants can be considered to control the drug release as confirmed by the drug release studies presented above. Finally, NO production was not observed in non-stimulated RAW 264.7 cells after DEX@DDS administration,

indicating that the formulations did not lead to an immune system activation (data not shown).

4. Conclusions

A continuous research effort to produce efficient nanocarriers for drug delivery is in progress to answer to the growing demand of innovative applications in medicine. In this work, we studied an exotic type of delivery systems characterized by a cubic structure, the so called cubosomes, which were for the first time formulated by combining GMO

with mannose esters. The cubic phase was maintained in the presence of the sugar-based surfactants at a concentration up to 10 mol% whereas a transition to a lamellar phase was observed at higher concentrations, regardless of the length and saturation of the acyl chain of the sugar esters. Instead, these latter parameters affected the fluidity of the systems, and the radius of the water channels present in the cubosomes thus modulating their release behaviour. Furthermore, the addition of sugar moieties to the prepared DDS formulations offers a viable strategy for active targeting to specific receptors. Showing a good cytocompatibility, the possibility to carry active molecules, and an increased activity of the loaded molecule, GMO/glycolipids nanoparticles represent an effective option to formulate and deliver drugs.

CRediT authorship contribution statement

Mattia Tiboni: Investigation, Formal analysis, Writing – original draft, Writing – review and editing; **Paola Astolfi:** Conceptualization, Investigation, Formal analysis, Writing – original draft, Writing – review and editing; **Michele Verboni:** Investigation, Formal analysis, Writing – original draft; **Serena Benedetti:** Investigation, Resources, Writing – original draft; **Elisabetta Giorgini:** Investigation, Formal analysis, Writing – original draft; **Valentina Notarstefano:** Investigation, Formal analysis, Writing – original draft; **Francesco Vita:** Investigation, Writing – review and editing; **Simone Ranieri:** Investigation; **Andrea Duranti:** Resources; **Simone Lucarini:** Resources; **Luca Casettari:** Conceptualization, Writing – review and editing; **Michela Pisani:** Conceptualization, Formal analysis, Investigation, Resources; Writing – original draft, Writing – review and editing, Project administration.

Declaration of Competing Interest

The authors declare that they have no known competing financial interests or personal relationships that could have appeared to influence the work reported in this paper.

Data availability

No data was used for the research described in the article.

Acknowledgments

Appendix A. Supporting information

Supplementary data associated with this article can be found in the online version at doi:10.1016/j.colsurfb.2023.113596.

References

[1] J.K. Patra, G. Das, L.F. Fraceto, E.V.R. Campos, M.D.P. Rodriguez-Torres, L. S. Acosta-Torres, L.A. Diaz-Torres, R. Grillo, M.K. Swamy, S. Sharma, S. Habtemariam, H.S. Shin, Nano based drug delivery systems: recent developments and future prospects, J. Nanobiotechnol. 16 (2018) 1–33, https://doi.org/10.1186/s12951-018-0392-8.
[2] T. Peng, W. Xu, Q. Li, Y. Ding, Y. Huang, Pharmaceutical liposomal delivery—specific considerations of innovation and challenges, Biomater. Sci. 11 (2022) 62–75, https://doi.org/10.1039/d2bm01252a.
[3] A. Angelova, V.M. Garamus, B. Angelov, Z. Tian, Y. Li, A. Zou, Advances in structural design of lipid-based nanoparticle carriers for delivery of macromolecular drugs, phytochemicals and anti-tumor agents, Adv. Colloid Interface Sci. 249 (2017) 331–345, https://doi.org/10.1016/j.cis.2017.04.006.
[4] S. Murgia, S. Biffi, R. Mezzenga, Recent advances of non-lamellar lyotropic liquid crystalline nanoparticles in nanomedicine, Curr. Opin. Colloid Interface Sci. 48 (2020) 28–39, https://doi.org/10.1016/j.cocis.2020.03.006.
[5] P. Astolfi, E. Giorgini, F.C. Adamo, F. Vita, S. Logrippo, O. Francescangeli, M. Pisani, Effects of a cationic surfactant incorporation in phytantriol bulk cubic phases and dispersions loaded with the anticancer drug 5-fluorouracil, J. Mol. Liq. 286 (2019) 110954, https://doi.org/10.1016/j.molliq.2019.110954.
[6] P. Astolfi, E. Giorgini, D.R. Perinelli, F. Vita, F.C. Adamo, S. Logrippo, M. Parlapiano, G. Bonacucina, S. Pucciarelli, O. Francescangeli, L. Vaccari, M. Pisani, Cubic and hexagonal mesophases for protein encapsulation: structural effects of insulin confinement, Langmuir 37 (2021) 10166–10176, https://doi.org/10.1021/acs.langmuir.1c01587.
[7] L.A. Maiorova, S.I. Erokhina, M. Pisani, G. Barucca, M. Marcaccio, O.I. Koifman, D. S. Salnikov, O.A. Gromova, P. Astolfi, V. Ricci, V. Erokhin, Encapsulation of vitamin B12 into nanoengineered capsules and soft matter nanosystems for targeted delivery, Colloids Surf. B Biointerfaces 182 (2019) 110366, https://doi.org/10.1016/j.colsurfb.2019.110366.
[8] S. Milak, A. Zimmer, Glycerol monooleate liquid crystalline phases used in drug delivery systems, Int. J. Pharm. 478 (2015) 569–587, https://doi.org/10.1016/j.ijpharm.2014.11.072.
[9] C.V. Kulkarni, W. Wachter, G. Iglesias-Salto, S. Engelskirchen, S. Ahualli, Monoolein: a magic lipid? Phys. Chem. Chem. Phys. 13 (2011) 3004–3021, https://doi.org/10.1039/c0cp01539c.
[10] J.C. Bode, J. Kuntsche, S.S. Funari, H. Bunjes, Interaction of dispersed cubic phases with blood components, Int. J. Pharm. 448 (2013) 87–95, https://doi.org/10.1016/j.ijpharm.2013.03.016.
[11] A. Yaghmur, O. Glatter, Characterization and potential applications of nanostructured aqueous dispersions, Adv. Colloid Interface Sci. 147–148 (2009) 333–342, https://doi.org/10.1016/j.cis.2008.07.007.
[12] C. Guo, J. Wang, F. Cao, R.J. Lee, G. Zhai, Lyotropic liquid crystal systems in drug delivery, Drug Discov. Today 15 (2010) 1032–1040, https://doi.org/10.1016/j.drudis.2010.09.006.
[13] A. Zabara, J.T.Y. Chong, I. Martiel, L. Stark, B.A. Cromer, C. Speziale, C. J. Drummond, R. Mezzenga, Design of ultra-swollen lipidic mesophases for the crystallization of membrane proteins with large extracellular domains, Nat. Commun. 9 (2018) 544, https://doi.org/10.1038/s41467-018-02996-5.
[14] H.M.G. Barriga, A.I.I. Tyler, N.L.C. McCarthy, E.S. Parsons, O. Ces, R.V. Law, J. M. Seddon, N.J. Brooks, Temperature and pressure tuneable swollen bicontinuous cubic phases approaching nature's length scales, Soft Matter 11 (2015) 600–607, https://doi.org/10.1039/c4sm02343a.
[15] A. Varki, Biological roles of glycans, Glycobiology 27 (2017) 3–49, https://doi.org/10.1093/glycob/cww086.
[16] H. Ghazarian, B. Idoni, S.B. Oppenheimer, A glycobiology review: carbohydrates, lectins and implications in cancer therapeutics, Acta Histochem. 113 (2011) 236–247, https://doi.org/10.1016/j.acthis.2010.02.004.
[17] V. Vill, R. Hashim, Carbohydrate liquid crystals: structure–property relationship of thermotropic and lyotropic glycolipids, Curr. Opin. Colloid Interface Sci. 7 (2002) 395–409, https://doi.org/10.1016/S1359-0294(02)00091-2.
[18] B.J. Boyd, C.J. Drummond, I. Krodkiewska, F. Grieser, How chain length, headgroup polymerization, and anomeric configuration govern the thermotropic and lyotropic liquid crystalline phase behavior and the air-water interfacial adsorption of glucose-based surfactants, Langmuir 16 (2000) 7359–7367, https://doi.org/10.1021/la991573w.
[19] P. Garidel, Y. Kaconis, L. Heinbockel, M. Wulf, S. Gerber, A. Munk, V. Vill, K. Brandenburg, Self-organisation, thermotropic and lyotropic properties of glycolipids related to their biological implications, Open Biochem. J. 9 (2015) 49–72, https://doi.org/10.2174/1874091×01509010049.
[20] G.C. Feast, T. Lepitre, N. Tran, C.E. Conn, O.E. Hutt, X. Mulet, C.J. Drummond, G. P. Savage, Inverse hexagonal and cubic micellar lyotropic liquid crystalline phase behaviour of novel double chain sugar-based amphiphiles, Colloids Surf. B: Biointerfaces 151 (2017) 34–38, https://doi.org/10.1016/colsurfb.2016.12.004.
[21] S. Khorshid, M. Montanari, S. Benedetti, S. Moroni, A. Aluigi, B. Canonico, S. Papa, M. Tiboni, L. Casettari, A microfluidic approach to fabricate sucrose decorated liposomes with increased uptake in breast cancer cells, Eur. J. Pharm. Biopharm. 178 (2022) 53–64, https://doi.org/10.1016/j.ejpb.2022.07.015.
[22] E. Crucianelli, P. Bruni, A. Frontini, L. Massaccesi, M. Pisani, A. Smorlesi, G. Mobbili, Liposomes containing mannose-6-phosphate-cholesteryl conjugates for lysosome-specific delivery, RSC Adv. 4 (2014) 58204–58207, https://doi.org/10.1039/c4ra08681c.
[23] V. Faivre, V. Rosilio, Interest of glycolipids in drug delivery: from physicochemical properties to drug targeting, Expert Opin. Drug Deliv. 7 (2010) 1031–1048, https://doi.org/10.1517/17425247.2010.511172.
[24] D.R. Perinelli, S. Lucarini, L. Fagioli, R. Campana, D. Vllasaliu, A. Duranti, L. Casettari, Lactose oleate as new biocompatible surfactant for pharmaceutical applications, Eur. J. Pharm. Biopharm. 124 (2018) 55–62, https://doi.org/10.1016/j.ejpb.2017.12.008.
[25] M. Verboni, D.R. Perinelli, C.Y. Qiu, M. Tiboni, A. Aluigi, S. Lucarini, J.K.W. Lam, A. Duranti, Synthesis and properties of sucrose- and lactose-based aromatic ester surfactants as potential drugs permeability enhancers, Pharmaceuticals 16 (2023) 223, https://doi.org/10.3390/ph16020223.
[26] M. Tiboni, E. Elmowafy, M.O. El-Derany, S. Benedetti, R. Campana, M. Verboni, L. Potenza, F. Palma, B. Citterio, M. Sisti, A. Duranti, S. Lucarini, M.E. Soliman, L. Casettari, A combination of sugar esters and chitosan to promote in vivo wound care, Int. J. Pharm. 616 (2022), 121508, https://doi.org/10.1016/j.ijpharm.2022.121508.
[27] M. Verboni, S. Lucarini, A. Duranti, 6′-O-lactose ester surfactants as an innovative opportunity in the pharmaceutical field: From synthetic methods to biological applications, Pharmaceuticals 14 (2021) 1306, https://doi.org/10.3390/ph14121306.

[28] S. Lucarini, L. Fagioli, R. Cavanagh, W. Liang, D.R. Perinelli, M. Campana, S. Stolnik, J.K.W. Lam, L. Casettari, A. Duranti, Synthesis, structure-activity relationships and in vitro toxicity profile of lactose-based fatty acid monoesters as possible drug permeability enhancers, Pharmaceutics 10 (2018) 81, https://doi.org/10.3390/pharmaceutics10030081.

[29] E. Elmowafy, M.O. El-Derany, F. Biondo, M. Tiboni, L. Casettari, M.E. Soliman, Quercetin loaded monolaurate sugar esters-based niosomes: sustained release and mutual antioxidant—hepatoprotective interplay, Pharmaceutics 12 (2020) 143, https://doi.org/10.3390/pharmaceutics12020143.

[30] S. Sarkar, B. Dyett, B. Lakic, A.S. Ball, L.Y. Yeo, J.F. White, S. Soni, C.J. Drummond, C.E. Conn, Cubosome lipid nanocarriers as a drug delivery vehicle for intracellular mycobacterium tuberculosis infections, ACS Appl. Mater. Interfaces 15 (2023) 21819–21829, https://doi.org/10.1021/acsami.3c00101.

[31] V.S. Madamsetty, R. Mohammadinejad, I. Uzieliene, N. Nabavi, A. Dehshahri, J. García-Couce, S. Tavakol, S. Moghassemi, A. Dadashzadeh, P. Makvandi, A. Pardakhty, A.A. Afshar, A. Seyfoddin, Dexamethasone: insights into pharmacological aspects, therapeutic mechanisms, and delivery systems, ACS Biomater. Sci. Eng. 8 (2022) 1763–1790, https://doi.org/10.1021/acsbiomaterials.2c00026.

[32] J.A. Arcos, M. Bernabé, C. Otero, Quantitative enzymatic production of 1,6-diacyl fructofuranoses, Enzym. Microb. Technol. 22 (1998) 27–35, https://doi.org/10.1016/S0141-0229(97)00100-2.

[33] Y. Watanabe, M. Miyawaki, S. Adachi, K. Nakanishi, R. Matsuno, Continuous production of acyl mannoses by immobilized lipase using a packed-bed reactor and their surfactant properties, Biochem. Eng. J. 8 (2001) 213–216, https://doi.org/10.1016/S1369-703X(01)00099-7.

[34] R. Campana, A. Merli, M. Verboni, F. Biondo, G. Favi, A. Duranti, S. Lucarini, Synthesis and evaluation of saccharide-based aliphatic and aromatic esters as antimicrobial and antibiofilm agents, Pharmaceuticals 12 (2019) 186, https://doi.org/10.3390/ph12040186.

[35] E. Aranda, I. García-Romera, J.A. Ocampo, V. Carbone, A. Mari, A. Malorni, F. Sannino, A. De Martino, R. Capasso, Chemical characterization and effects on Lepidium sativum of the native and bioremediated components of dry olive mill residue, Chemosphere 69 (2007) 229–239, https://doi.org/10.1016/J.CHEMOSPHERE.2007.04.026.

[36] S. Catalani, F. Palma, S. Battistelli, B. Nuvoli, R. Galati, S. Benedetti, Reduced cell viability and apoptosis induction in human thyroid carcinoma and mesothelioma cells exposed to cidofovir, Toxicol. Vitr. 41 (2017) 49–55, https://doi.org/10.1016/j.tiv.2017.02.008.

[37] M. Verboni, M. Sisti, R. Campana, S. Benedetti, F. Palma, L. Potenza, S. Lucarini, A. Duranti, Synthesis and biological evaluation of 6-o-sucrose monoester glycolipids as possible new antifungal agents, Pharmaceuticals 16 (2023) 136, https://doi.org/10.3390/ph16020136.

[38] M. Pisani, L. Quassinti, M. Bramucci, R. Galassi, F. Maggi, B. Rossi, A. Damin, P. Carloni, P. Astolfi, Nanostructured liquid crystalline particles as delivery vectors for isofuranodiene: characterization and in-vitro anticancer activity, Colloids Surf. B Biointerfaces 192 (2020), 111050, https://doi.org/10.1016/j.colsurfb.2020.111050.

[39] C. Fong, T. Le, C.J. Drummond, Lyotropic liquid crystal engineering–ordered nanostructured small molecule amphiphile self-assembly materials by design, Chem. Soc. Rev. 41 (2012) 1297–1322, https://doi.org/10.1039/c1cs15148g.

[40] J. Briggs, H. Chung, M. Caffrey, The temperature-composition phase diagram and mesophase structure characterization of the monoolein/water system, J. Phys. II. 6 (1996) 723–751, https://doi.org/10.1051/jp2:1996208.

[41] L.B. Rodrigues, H.F. Leite, M.I. Yoshida, J.B. Saliba, A.S.C. Junior, A.A.G. Faraco, In vitro release and characterization of chitosan films as dexamethasone carrier, Int. J. Pharm. 368 (2009) 1–6, https://doi.org/10.1016/j.ijpharm.2008.09.047.

[42] K. Krukiewicz, M. Chudy, S. Gregg, M.J.P. Biggs, The synergistic effects of gold particles and dexamethasone on the electrochemical and biological performance of PEDOT neural interfaces, Polymers 11 (2019) 67, https://doi.org/10.3390/polym11010067.

[43] Q. Zhou, Y. Yang, J. Ni, Z. Li, Z. Zhang, Rapid recognition of isomers of monochlorobiphenyls at trace levels by surface-enhanced Raman scattering using Ag nanorods as a substrate, Nano Res. 3 (2010) 423–428, https://doi.org/10.1007/s12274-010-0001-0.

[44] M. Marchetti, M. Offroy, F. Abdat, P. Branchu, P. Bourson, C. Jobard, J.F. Durmont, G. Casteran, Chemometrics-assisted monitoring in Raman spectroscopy for the biodegradation process of an aqueous polyfluoroalkyl ether from a fire-fighting foam in an environmental matrix, Environ 7 (2020) 1–14, https://doi.org/10.3390/environments7010004.

[45] T. Lemma, F. De Barros Souza, C.A.T. Soto, A.A. Martin, An FT-Raman, FT-IR, and Quantum Chemical Investigation of Stanozolol and Oxandrolone, 8 (2018) 2, https://doi.org/10.3390/bios8010002.

[46] A.C.S. Talari, Z. Movasaghi, S. Rehman, I.U. Rehman, Raman spectroscopy of biological tissues, Appl. Spectrosc. Rev. 50 (2015) 46–111, https://doi.org/10.1080/05704928.2014.923902.

[47] D.A. Long. Infrared and Raman characteristic group frequencies Tables and charts, 3rd Edition, George Socrates John Wiley and Sons, Ltd, Chichester, 2001.

[48] X. Cai, B. Fan, S.H. Thang, C.J. Drummond, N. Tran, J. Zhai, Paclitaxel-loaded cubosome lipid nanocarriers stabilised with pH and hydrogen peroxide-responsive steric stabilisers as drug delivery vehicles, J. Mater. Chem. B 11 (2023) 403–414, https://doi.org/10.1039/D2TB01530G.

[49] G.M. Pontes-Quero, L. Benito-Garzón, J. Pérez Cano, M.R. Aguilar, B. Vázquez-Lasa, Modulation of inflammatory mediators by polymeric nanoparticles loaded with anti-inflammatory drugs, Pharmaceutics 13 (2021) 1–21, https://doi.org/10.3390/pharmaceutics13020290.